

N 64 33681
FACILITY FORM 502
(ACCESSION NUMBER)
20
(PAGES)
TMX-54787
(NASA CR OR TMX OR AD NUMBER)

(THRU)
1
(CODE)
18
(CATEGORY)

CORROSION OF MATERIALS BY REFLUXING MERCURY AT TEMPERATURES ABOVE 1000°F

by

Coulson M. Scheuermann

Charles A. Barrett

Warren H. Lowdermilk

Louis Rosenblum

National Aeronautics and Space Administration

Lewis Research Center, Cleveland, Ohio

OTS PRICE

XEROX \$ 1.00 FS
MICROFILM \$ 0.50 mfl

To be presented at the Washington Meeting of The Electrochemical Society,
October 11 - 15, 1964, at the Sheraton-Park Hotel, Washington, D. C.

TMX # 54787

ABSTRACT

33681

Corrosion of Materials by Refluxing Mercury at Temperatures Above 1000°F

by

Coulson M. Scheuermann

Charles A. Barrett

Warren H. Lowdermilk

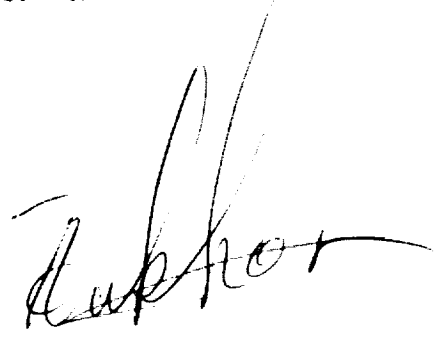
Louis Rosenblum

The compatibility of various materials with mercury was determined for their possible use in contemporary space turbo-electric power systems.

Twenty-four materials were selected for testing from the following categories: austenitic stainless steels, martensitic chromium steels, cobalt base alloys, nickel base alloys, and refractory metals and alloys.

Test results and materials are discussed with respect to compatibility, strength, and development problems associated with space systems.

Corrosion rates were determined for several alloys. These are discussed and compared with existing theory.

A handwritten signature in dark ink, appearing to read 'Luphor', is located in the bottom right corner of the page.

INTRODUCTION

A test program was initiated at the NASA Lewis Research Center to study the compatibility of materials with mercury for their possible use as containment materials in space turbo-electric power systems. The selection of test alloys is given, with their compositions and availability status, in figure 1. Twenty-four materials were selected. These were chosen from the categories of austenitic stainless steels, martensitic chromium steels, cobalt base alloys, nickel base alloys, and refractory metal base alloys. Previous work on mercury corrosion had shown that alloys of high nickel content were especially subject to mercury corrosion. Therefore, a major criterion for selecting materials for this program was that they had a low nickel content. Nickel base alloys were included for comparison purposes.

The reflux capsule method was chosen for the testing because it was relatively inexpensive, it was a severe test and should lend itself easily to a rating of materials, and it was hoped to be a method which would closely simulate the expected conditions in the boiler; i.e., heavy solution attack and deposit build-up. The temperatures of the tests were chosen to bracket the expected boiler temperatures in the Snap-6 system and

were 1000° to 1300°F. Test times were chosen at intervals up to 5000 hours.

PROCEDURE

The mercury corrosion capsules, figure 2, were machined from bar stock to $\frac{1}{2}$ -inch C.D., 1 $\frac{3}{4}$ inches long, and 0.040-inch wall thickness. The capsules were cleaned, filled to $\frac{1}{3}$ total internal volume, and sealed with an electron beam welder. They were heated to temperature in beds of individual furnaces, figures 3 and 4. Upon completion of the tests, the capsules were pierced for draining of the mercury from the capsules.

Residual mercury was removed by vacuum distillation. The capsules were sectioned lengthwise and one section mounted and examined metallographically.

Depths of penetration by the mercury were measured with a filar eyepiece at the points of deepest penetration. Capsules of particular interest were examined with an electron beam microprobe.

RESULTS AND DISCUSSION

In general, the sectioned capsules showed complete "tinning" by the mercury. However, the martensitic chromium steels at the lower temperatures showed only partial "tinning" and the refractory metals were characterized by no "tinning" at the lower temperatures and only partial "tinning" at the

higher temperatures. Those capsules in which a high degree of "turning" occurred also showed a crystalline deposit at the boiling interface which varied greatly in amount with the varying test conditions.

Figure 5 compares the maximum penetrations observed in selected alloys after 5000 hours at temperature. All materials were tested for 300 hours; however, due to limited testing facilities and time, representative or interesting alloys of each material category, except nickel base alloys, were chosen for testing at longer times. From this figure the materials can be listed in order of decreasing corrosion resistance as follows: Cb-12r and tantalum, Sicromo 9M, AV-350, and HS-25. This order is assumed to be that of their respective material categories also. The anomaly of the observed negative temperature coefficient for type 304 stainless steel is at present unresolved and under investigation. This behavior is believed to be typical of the 18-8 stainless steels.

The mechanisms which may determine the rate of corrosion can be presented as in figure 6. Solid state diffusion ordinarily would not play a significant part in the corrosion process. This leaves the solution rate and the rate of diffusion across the boundary layer as possible rate

controlling steps in the case where there is only a thin boundary layer separating the liquid stream from the solid surface. As shown at the bottom of the figure, there is also the possibility of liquid diffusion being the rate controlling step in some cases.

When the amount of corrosion is plotted against time on log-log scales, solution rate controlled and boundary layer diffusion controlled processes should be distinguishable from liquid diffusion controlled processes, since, ideally, the former should yield lines with slopes of 1.0, while the latter should yield lines with slopes of 0.5.

An example of a linear corrosion rate is shown in figure 7. Here we see the corrosion of Hastelloy B as maximum penetration in mils plotted against time in hours on log-log scales. Hastelloy B contains approximately 66% by weight of the highly mercury-soluble element, nickel. The remaining elements, iron and molybdenum, would not be expected to form an integral insoluble network because of their high solubilities in nickel. The absence of such a network would permit ready access of the mercury stream to the receding solid nickel surface, giving a solution controlled, or boundary layer controlled, corrosion rate.

When the highly mercury-soluble element is not the major constituent of the alloy, or when the insoluble elements can form a residual network, permitting the formation of quiescent liquid channels between the solid-liquid reaction front and the mercury stream, diffusion through the quiescent liquid can be the controlling rate. Figure 8 shows the corrosion of Sicromo 9M in both mils of penetration and weight loss in mg/cm^2 plotted against time. The weight loss figures were calculated from the penetration data and electron beam microprobe analysis data. At 1000°F up to 5000 hours and 1100°F up to 2000 hours, the rate is linear. Metallographic results in this range showed relatively shallow and direct penetrations as indicated in the photomicrograph to the upper left. From 2000 to 5000 hours at 1100°F and at 1200°F diffusion is the controlling rate. Here metallographic results showed a long, or tortuous, path for the penetrations as shown at the lower left which could give a quiescent liquid layer.

If the insoluble network reaches a critical thickness where the internal stresses created by the change in volume due to the corrosive attack reaches the critical shear stress for this network, cracks will be initiated in the network. These cracks conceivably could give the mercury

stream ready access to local regions of solid base metal. If this happens, a change from parabolic to linear behavior could be expected. Reversion to parabolic behavior, however, would not be expected because the cracks would have already been initiated and should continue to grow as the corrosion continues. Spalling of this corrosion product layer, or network, would be expected.

This seems to be a plausible explanation of what is observed with the alloys H-8187 and HS-25. Figure 9 shows such cracking and spalling of the corrosion layer in an HS-25 capsule which had been tested at 1300°F for 5000 hours.

Figure 10 is the weight loss - time curves for H-8187. The capsules at 1100°F up through 2000 hours did not show cracking of the corrosion layer. At 5000 hours the cracks appeared, so the transition to linear behavior is likely near 5000 hours. All capsules at 1200°F and 1300°F , except those run for 300 hours, showed cracking of this layer; therefore, the transitions may be expected near the points indicated.

The HS-25 weight loss data are presented in figure 11. At 1300°F all capsules showed cracking of the corrosion layer. At 1200°F only the 300-

hour capsules showed no cracking. The 300- and 1000-hour capsules at 1100°F did not show cracking, while those at longer times did.

CONCLUSIONS

In conclusion, materials can be listed in order of decreasing corrosion resistance as follows: refractory metals and alloys, martensitic chromium steels, austenitic stainless steels, cobalt base alloys, and finally nickel base alloys.

The rate of corrosion of a material in mercury can be expected to be a linear function of time, provided there is no formation of an integral, relatively insoluble, network as a result of the corrosion process which might permit the maintenance of a quiescent liquid layer. If such a layer were formed, the corrosion rate would become parabolic. If this network were brittle and cracks were initiated in it, the corrosion rate would again become linear; however, a reversion back to parabolic behavior would not be expected.

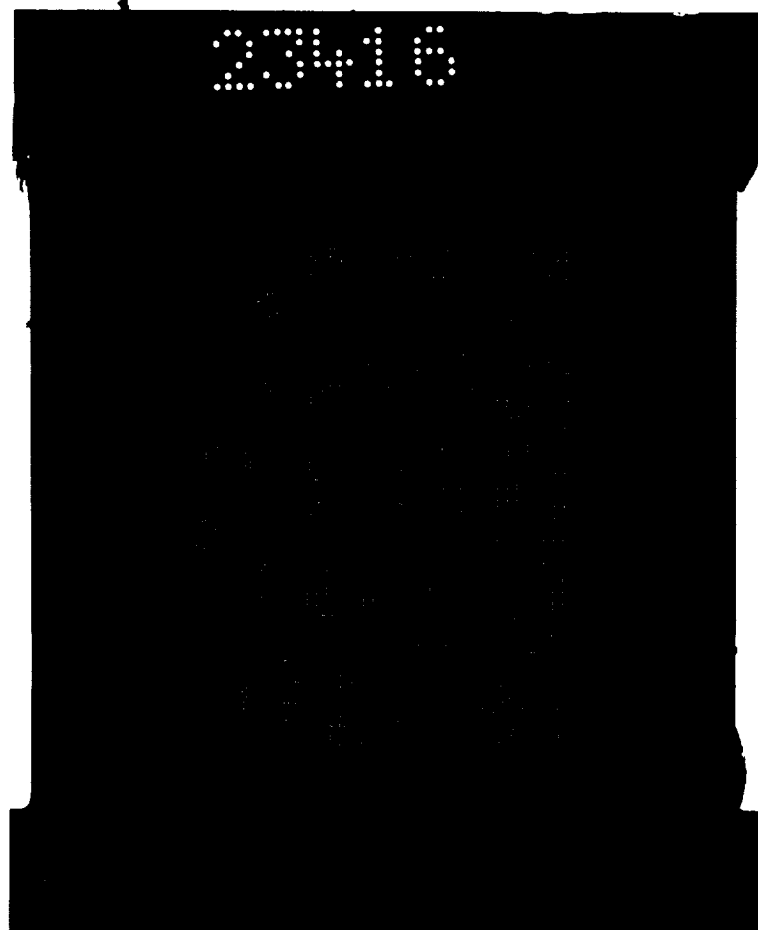


Figure 1

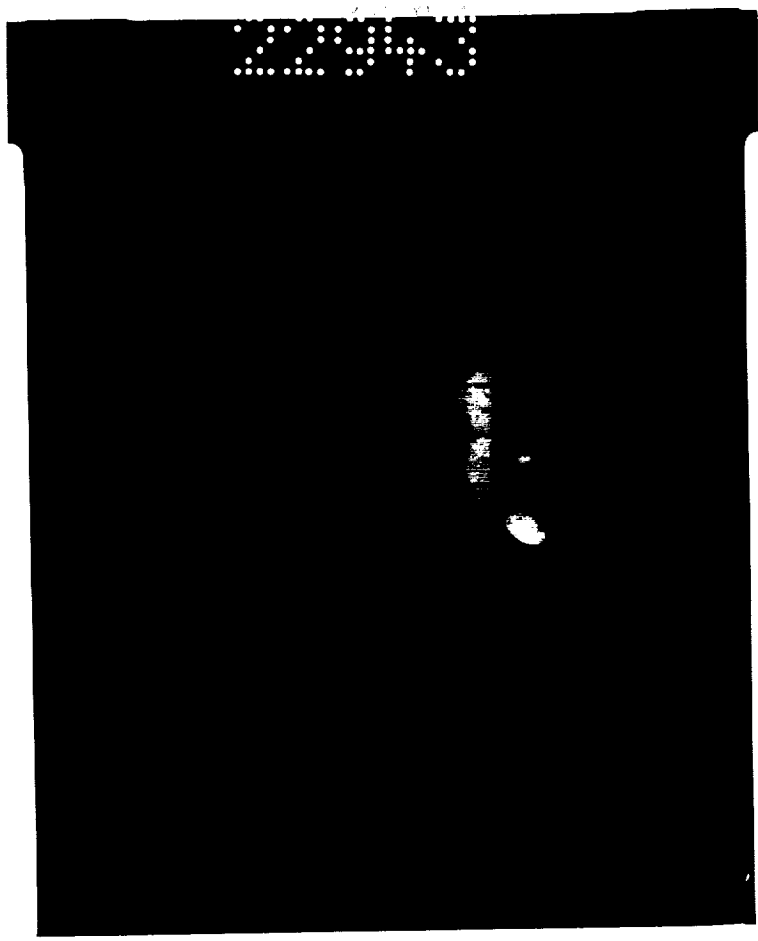


Figure 2

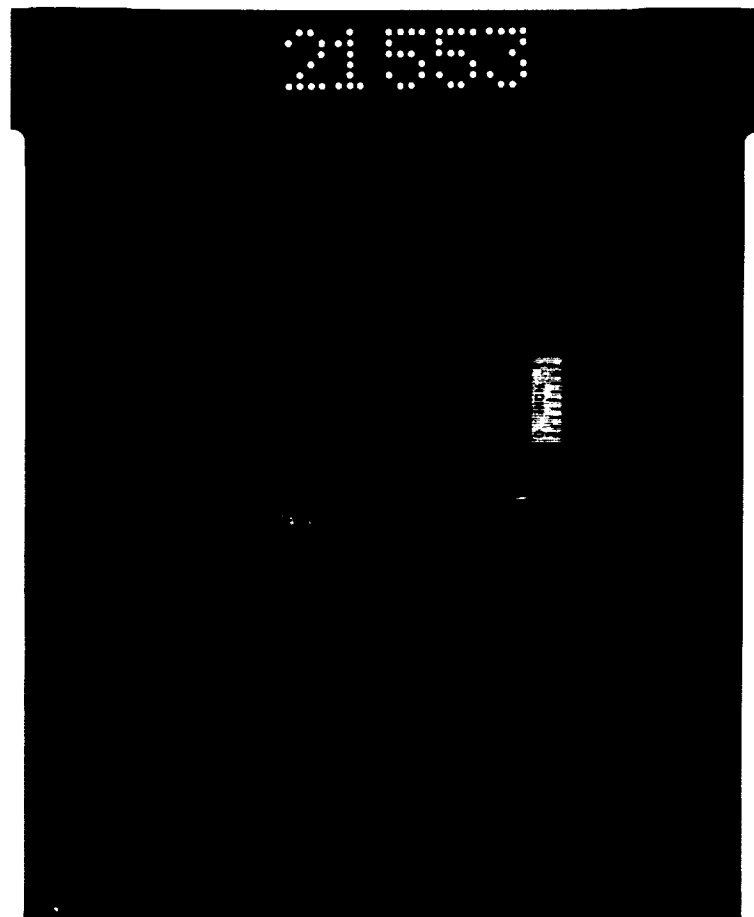


Figure 3

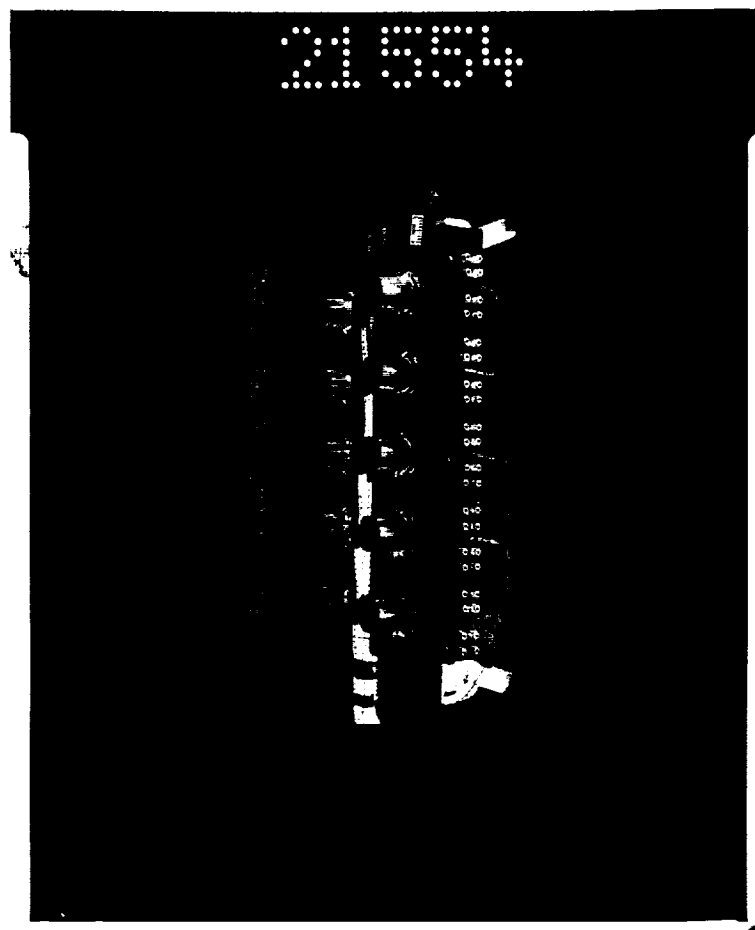


Figure 4

MAXIMUM PENETRATION, MILS

389 71
RESEARCH
PITTING

100

10

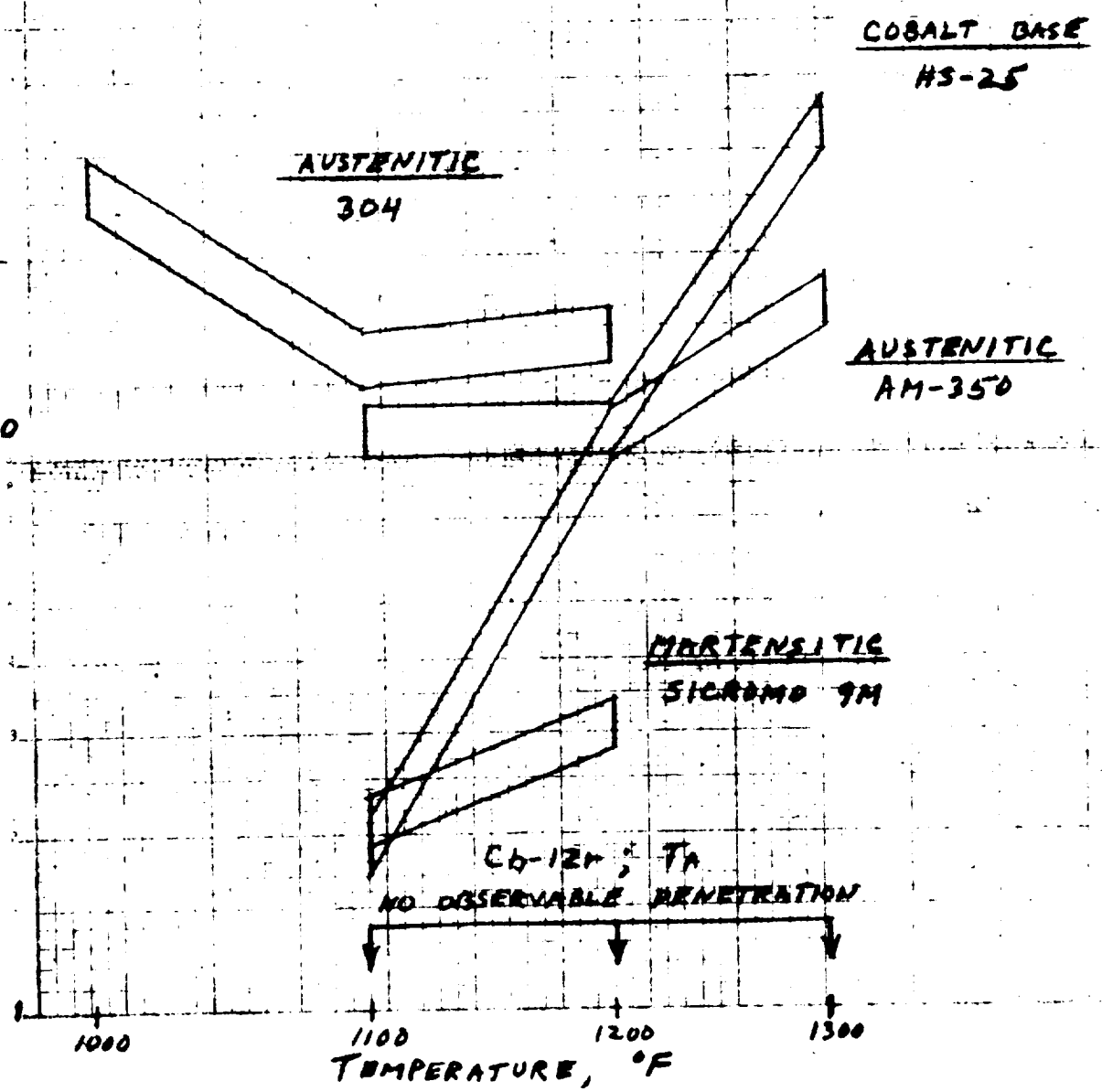


Figure 5

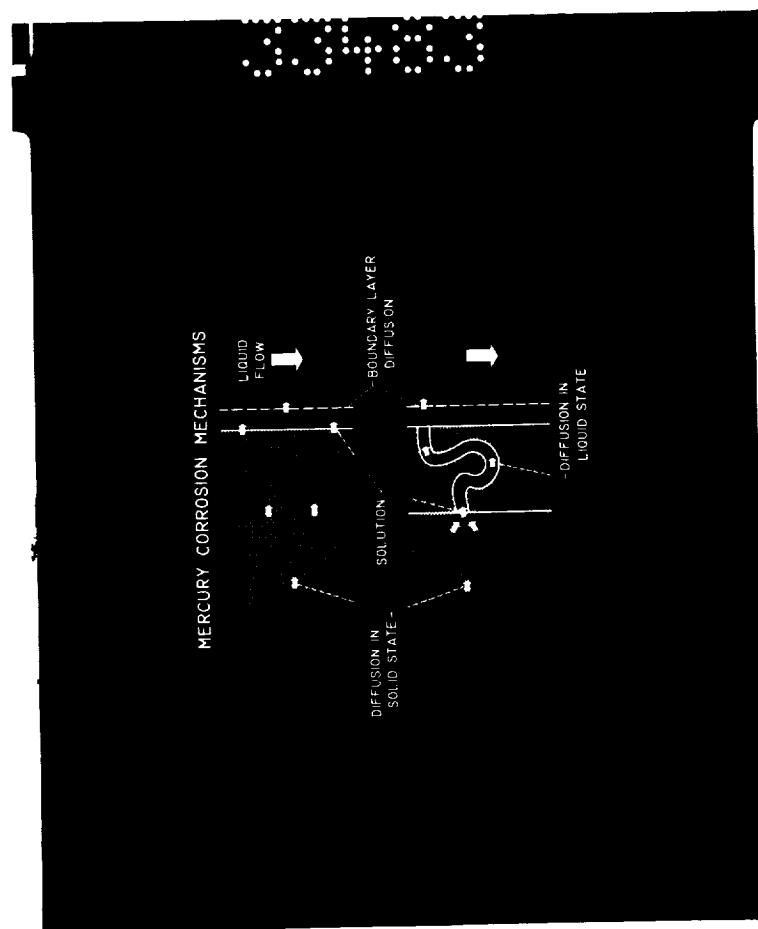


Figure 6

CORROSION OF HASTELLOY B BY MERCURY

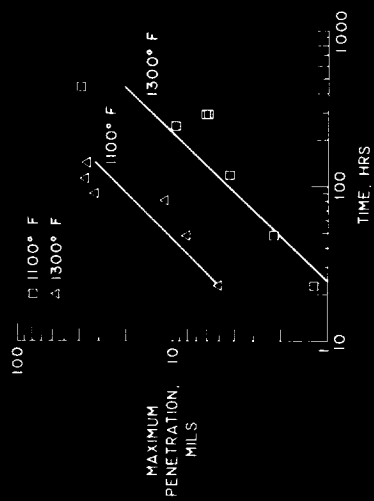


Figure 7

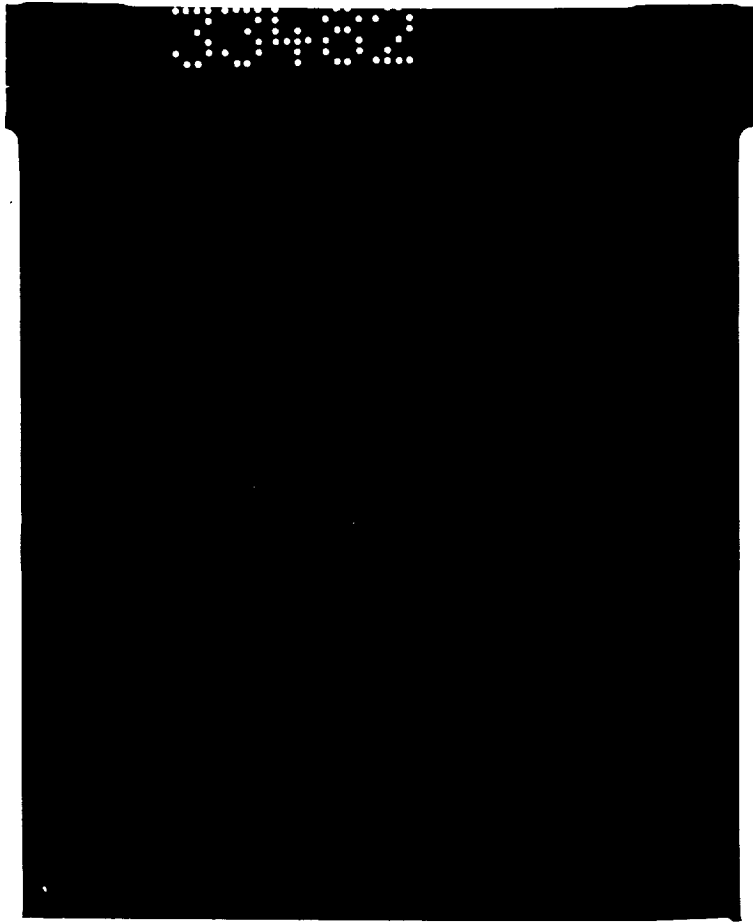


Figure 8

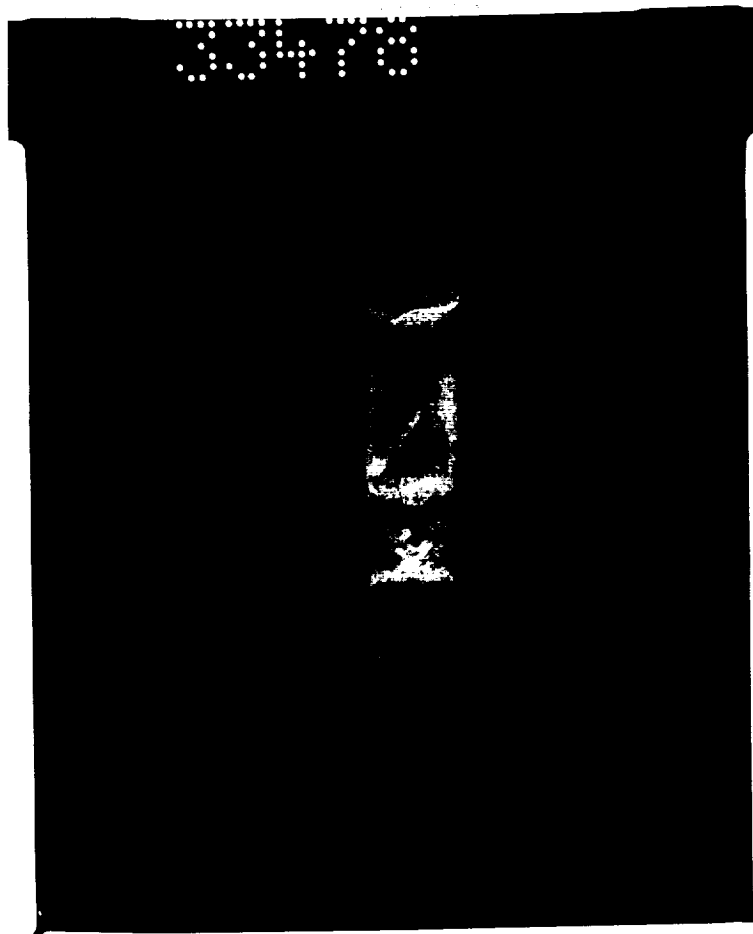


Figure 9

1000

CORROSION OF H-8187 BY MERCURY

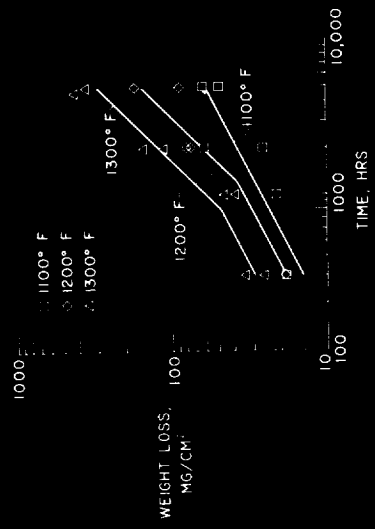


Figure 10

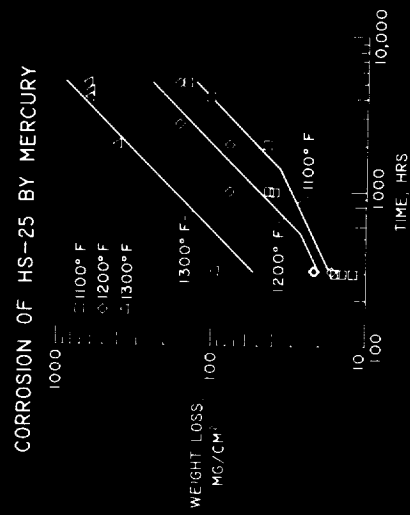


Figure 11